View metadata, citation and similar papers at core.ac.uk

brought to you by CORE

provided by Publications of the IAS Fellows

J Mater Sci: Mater Electron
DOI 10.1007/s10854-010-0189-5

Structural and electrical studies on $Bi_2VO_{5.5}/Bi_4Ti_3O_{12}$ multilayer thin films

Neelam Kumari · S. B. Krupanidhi · K. B. R. Varma

Received: 16 June 2010 / Accepted: 9 August 2010
© Springer Science+Business Media, LLC 2010

Abstract The textured multilayer (ML) thin films of bismuth layered ferroelectric (FE) compounds, $Bi_2VO_{5.5}$ (BVO) and $Bi_4Ti_3O_{12}$ (BTO) with different individual layer thicknesses were fabricated via pulsed laser deposition technique on Pt(111)/TiO_2/SiO_2/Si substrates. X-ray diffraction studies confirmed that BVO and BTO retained their respective crystal structures in these multilayer (ML) thin films. The atomic force microscopy and scanning electron microscopy studies showed smooth and dense microstructures. The polarization hysteresis (P–E) studies on a representative (BVBT30) ML thin film at 300 K confirmed the remnant polarization ($2P_r$) and coercive field (E_c) to be $\sim$20 μC/cm^2 and 250 kV/cm, respectively. The value of P_r obtained was greater than that of the single layer thin film of BVO ($P_r \sim 5.6$ μC/cm^2). The room temperature dielectric constant (ε_r') and the loss (D) for BVBT30 ML measured at 100 kHz were 170 and 0.01, respectively. The frequency and temperature dependent dielectric constant, impedance, modulus and ac conductivity of these ML thin films were studied as a function of frequency (100 Hz–1 MHz) in the 25–300 °C temperature range. Two distinct electrical responses were observed in these films, which were attributed to the grain effects at low temperatures and grain boundary effects at higher temperatures. The frequency dependent electrical conductivity was fitted well with the double power law which evidenced two different types of contributions to the conductivity; the low frequency conductivity being due to the short range translational hopping and the high frequency conductivity was due to the localized or reorientational hopping.

N. Kumari · S. B. Krupanidhi · K. B. R. Varma (✉)
Materials Research Center, Indian Institute of Science,
Bangalore 560012, India
e-mail: kbrvarma@mrc.iisc.ernet.in

1 Introduction

Fabrication and stabilization of special/artificial structures that do not occur naturally has been the current interest of study in materials research [1]. The control of properties could be achieved by tailoring the lattices [2] e.g. by lattice mismatch induced interface-strain engineering, polarization mismatch enhancing polarization, chemical heterogeneity, which in turn introduces spatial fluctuation in dipole moment effectively. The Multilayers (ML) and artificial superlattices, which are composed of thin layers of two or more different structural materials stacked in a well designed sequence may result in the enhancement of physical properties or may exhibit remarkably different properties which do not exist in either of their parent compounds [3–6]. Average physical behavior of the MLs/superlattice depends mainly on the interfacial coupling among the layers and size of the individual layers. Many other factors such as surface morphology, interface structure between the sublayers and the substrate, lattice mismatch and the difference in the thermal expansion coefficients of the constituent materials also influence the physical behavior of the overall ML structure.

Bismuth vanadate [$Bi_2VO_{5.5}$, (BVO)] crystalline phase, which is an $n = 1$ member of the Aurivillius family of oxides with intrinsic oxygen vacancies in the perovskite layer [7–9] possesses coexistence of polar response [7, 10] and high ionic mobility [11] which is generally incompatible in most ferroelectric materials. On the other hand bismuth titanate [$Bi_4Ti_3O_{12}$ (BTO)], which is an $n = 3$ member of Aurivillius family has been reported to be a promising ferroelectric and electro-optic material [12–15]. BTO-BVO solid solution was reported to possess better ferroelectric properties and low leakage current than that of the single BVO [16]. Since the multilayer thin films

Published online: 21 August 2010

provide a better opportunity to engineer the material properties over the composite bulk or homogeneous thin film because of interesting contributions arising from the interfaces, the MLs of BVO and BTO were fabricated and characterized for various physical properties. In the present work the MLs consisting of BVO and BTO were fabricated and studied their physical properties.

2 Experimental

In this study, the BVO and BTO layers were stacked alternatively by a multitarget-pulsed laser deposition technique on platinized silicon substrate, Pt(111)/TiO_2/SiO_2/Si(100). A 248 nm excimer laser (Lambda Physik Compex 201) operated at 5 Hz was alternately focused onto the well-sintered freshly polished BVO and BTO rotating target with an energy density of 2 Jcm^{-2} at an angle of 45° by a UV lens. The substrates were placed parallel to the targets at a distance of 3.5 cm and heated to 650 °C by a resistance heater. The chamber was first pumped down to 1×10^{-6} m bar, and then high purity oxygen was introduced using a mass flow controller to obtain oxygen partial pressure of 100 m Torr. After deposition of the designed number of layers, the samples were cooled down to room temperature under an oxygen pressure of 1 m bar to minimize the oxygen ion vacancies. Fabricating single layers followed by cross sectional scanning electron microscopy (SEM) (Sirion 200) facilitated the optimization of the growth rate per pulse for BVO and BTO. The growth rate under similar deposition conditions are the same for the BVO and BTO, thus one would expect the same thickness for all the ML thin films prepared by the same number of laser shots (pulses). The X-ray diffraction (XRD) studies were carried out to identify the phase and crystallographic structure of the ML films using Cu K_α ($\sim$1.541 Å) radiation (Scintag XR2000 Diffractometer). The surface morphology of these ML films was examined by means of contact mode atomic force microscope (AFM) (Veeco CP-II). SEM was employed to study the microstructural texture of the films. For electrical measurements, gold dots of 1.96×10^{-3} cm^2 area were deposited on the top surface of the films through a shadow mask and thermal evaporation technique. The Pt surface was used as the bottom electrode for capacitance measurements. A HP4294A impedance analyzer was used for the conventional dielectric measurement. The dielectric constant and ac electrical conductivity measurements were performed as a function of frequency (100 Hz–1 MHz) at various temperatures (25–350 °C), at signal strength of 0.5 V. The polarization–electric field (P–E) hysteresis behavior was studied using a Precision Workstation (Radiant Technologies, Inc.) ferroelectric test system in virtual ground mode.

3 Results and discussion

3.1 Structure and microstructure

The MLs with four different stacking thicknesses ($t \sim 10$, 20, 30 and 40 nm) were fabricated with a total thickness of $\sim$350 nm by PLD technique. The stacking thickness (t) is defined as the combined thickness of a BVO and a BTO layer as indicated schematically in Fig. 1a. All ML structures were fabricated under the same optimized deposition conditions as used for the fabrication of BVO and BTO single layer films. In all the ML structures, equal thicknesses of BVO and BTO individual layers were maintained by optimizing the single layer thickness. Multilayered thin films are abbreviated as BVBT t, where the number t is the total thickness of one stack i.e. one layer of BVO and one layer of BTO in nm. The XRD pattern of BVBT ML thin films is depicted in Fig. 1b along with the magnified view (Fig. 1c) of the (002) reflection of BVO. The appearance of only (*00l*) peaks of both BVO and BTO in the diffraction pattern confirms the grain oriented growth (textured) of the ML structures. Further, it is clear from Fig. 1c that there is a shift in the (002) peak position towards lower 2θ with increasing stacking thickness suggesting an increase in out of plane lattice parameter of BVO in these multilayers which may be due to the lattice mismatch between the individual layers and with the substrate. Both BTO

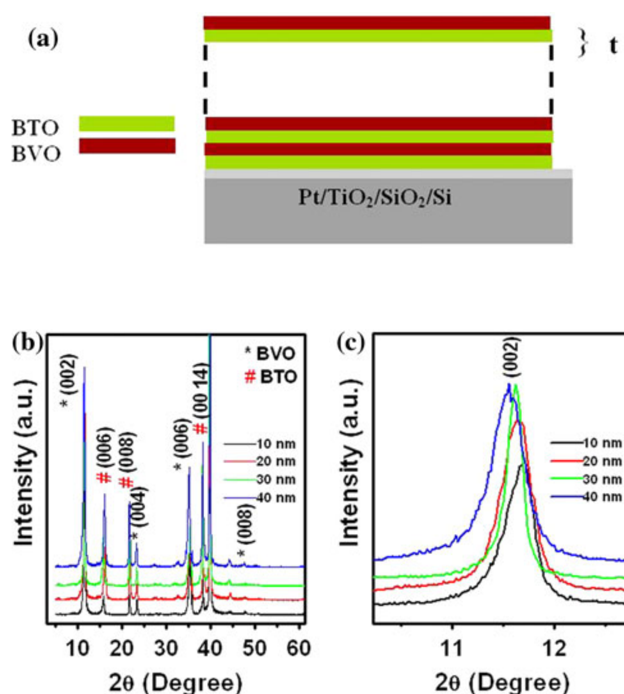

Fig. 1 **a** Schematic of a BVBT Multilayer thin film. **b** X-Ray diffraction patterns of BVBT Multilayers with different stacking thicknesses. **c** The magnified view of the (002) reflection of BVO

($a = 5.410$ Å) and BVO ($a = 5.543$ Å) have respective lattice mismatches of −0.09% and −2.487% with face diagonal of Pt ($a = 3.923$ Å) and therefore experience compressive in-plane stress. The lattice mismatch between BTO and BVO in *ab* plane is around 3%, which would give rise to a significant interfacial strain in the MLs as these two materials stacked one over the other which may be accounted for the shift in the 2θ values.

AFM was used to analyze the surface morphology and roughness of BVBT ML films. Figure 2a–d shows the contact mode AFM images of BVBT ML thin films. In all the cases (a–d) the BVBT ML film surface morphology is characterized by particle-like features of about 200–400 nm (often clustered) in size which were packed tightly resulting in high density structures. However the particle size increases slightly with the increase of stacking thickness of

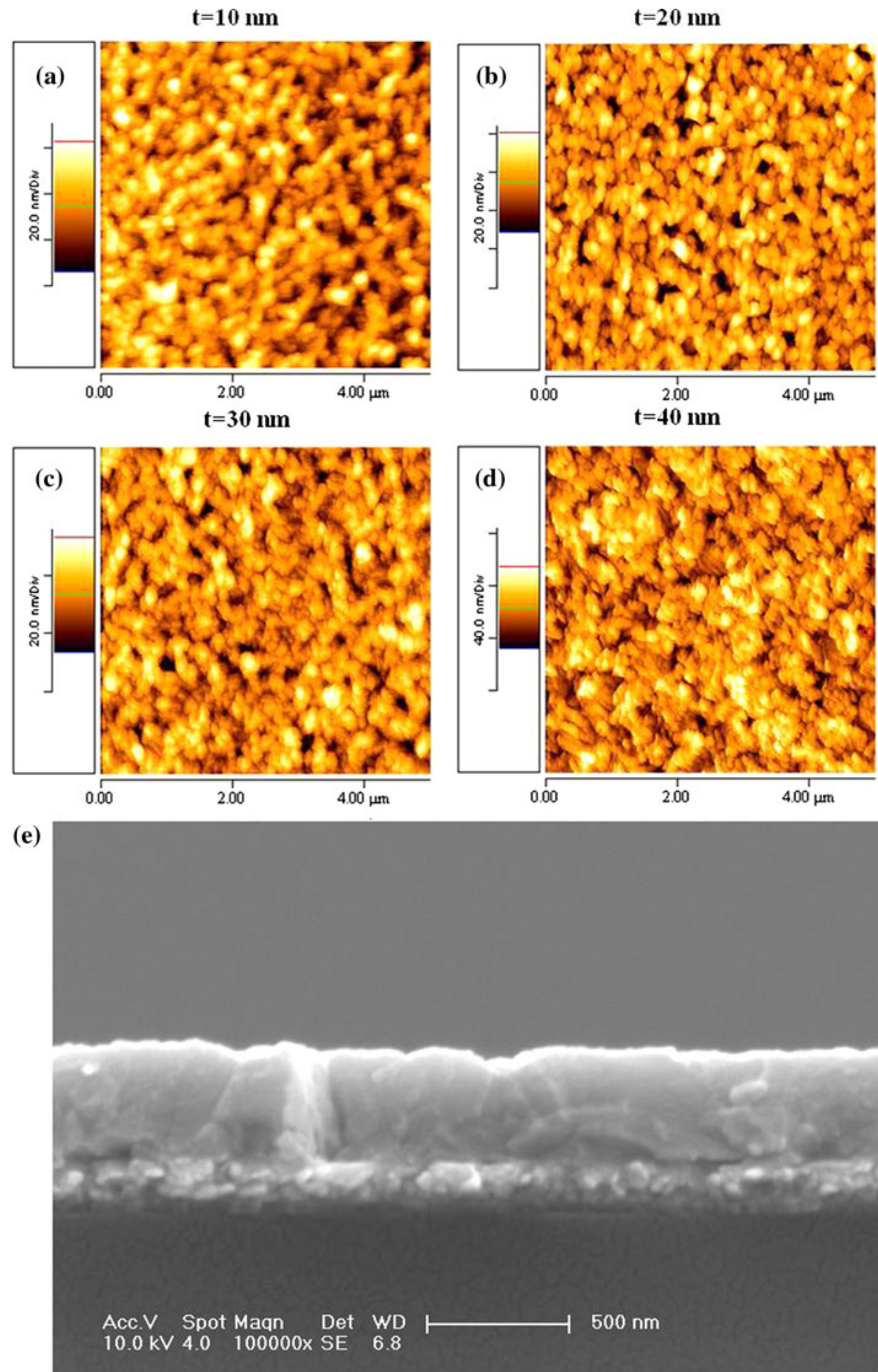

Fig. 2 **a–d** AFM micrograph showing surface topography of BVBT multilayer thin film. **e** Cross-sectional scanning electron micrograph of representative BVBT multilayer thin film

the multilayer film. The line profile of the surfaces indicate a smooth morphology with rms roughness of ~4 nm for BVBT 20 ML film. The surface roughness increased with the stacking thickness from 4 nm for BVBT 10–8 nm for BVBT40. As the number of interfaces decreases with periodicity for BVBT40 film, the individual layers get enough time to relax and the surface becomes more and more rough. The cross-sectional microstructure of these ML films was studied by SEM. Figure 2e shows the SEM micrograph of the representative BVBT20 ML film. It revealed a dense microstructure with sharp interface at the substrate indicating the coherent growth of the ML. The thicknesses of these MLs as determined from cross sectional SEM micrographs were in the range of 340–350 nm as expected.

3.2 Ferroelectric studies

The ferroelectric (FE) nature of the BVBT ML thin films was confirmed at room temperature based on the polarization hysteresis (P–E) measurement. BVBT ML with different stacking thicknesses were fabricated to study the interfacial coupling between the individual layers of these MLs thin film. The P–E response of one of the multilayer thin films with a stacking thickness of 30 nm is depicted in Fig. 3a as a function of applied electric field. These P–E hysteresis loops have been obtained at a switching frequency of 1 kHz. Well defined P–E loops obtained at a higher electric field (~940 kV/cm) confirm the intrinsic ferroelectric nature of these ML thin films. At the applied voltage of 35 V and probing frequency of 1 kHz, the measured values of remnant polarization ($2P_r$) and coercive field (E_c) for BVBT30 ML thin films were ~20 μC/cm^2 and 232 kV/cm, respectively. It is to be noted that this value of remnant polarization is higher than that reported for the single layer BVO thin films [17] deposited on platinized silicon substrate. However it is lower than that a single layer of polycrystalline BTO thin films [18, 19]. In order to investigate the effect of extrinsic contribution to the ferroelectric properties of BVBT ML thin film, the frequency dependence of the P–E loops of these films was studied. The P–E loops of BVBT 30 ML thin films were measured at different frequencies ranging from 500 Hz to 2 kHz. Figure 3b shows the P–E loops of BVBT 30 ML thin film measured at different frequencies and at an applied field of 920 kV/cm. Similar behavior was observed for the other BVBT ML thin films. These studies further suggest that the observed P–E loops show a weak frequency dependence which might be due to the space charges accumulated at the interfaces contributing to the non remnant polarization in these multilayer structures. To verify this fact we have performed the pulsed polarization experiment (PUND) on these samples. Figure 3c shows the polarization characteristics as a function of applied voltage obtained from PUND measurement on BVBT 30 thin film with a pulse width of 1 ms and pulse delay of 1,000 ms. It is observed that P*, −P*, dP and −dP obtained from PUND measurements gradually became flat with increasing voltage approaching near saturation. For an ideal FE sample the value of dP (or −dP), which in a sense represents only the remnant (true) polarization of the material investigated, should be equal to the value of total remnant polarization ($2P_r$) from the P–E hysteresis measurement [20]. In the present case, the value of dP obtained for BVBT30 in PUND measurement at an applied voltage of 35 V was 4 μC/cm^2, whereas the $2Pr$ value obtained from the PE hysteresis measured at 35 V was ~20 μC/cm^2. This huge difference in polarization values in ML thin films may be resulting from the large number of charge defect states at the interfaces present which in turn may be a possible source of non remnant polarization contribution to the observed P–E loops in the hysteresis measurements. Further, the leakage current in these multilayer thin films could be another factor partially accounting for the deviation from the ideal dP = $2P_r$ behavior.

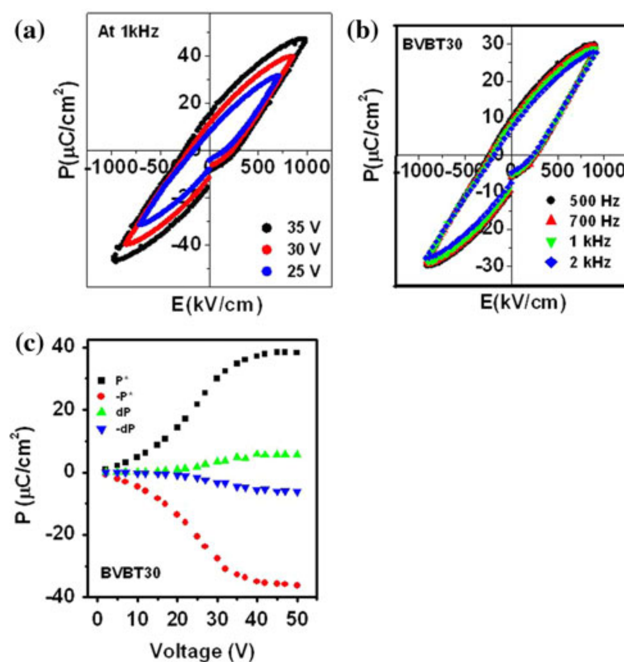

Fig. 3 P–E response of a BVBT30 multilayer thin film as a function of **a** applied voltage **b** probing frequency. **c** PUND measurements carried on BVBT30 ML thin film at different applied voltages

Figure 4a–c shows the room temperature P–E behavior of BVBT ML films of different stacking thicknesses. These P–E hysteresis loops have been obtained at a probing frequency of 1 kHz under the same maximum applied electric field of 920 kV/cm. The nature of the P–E hysteresis loops obtained established the intrinsic ferroelectric nature of

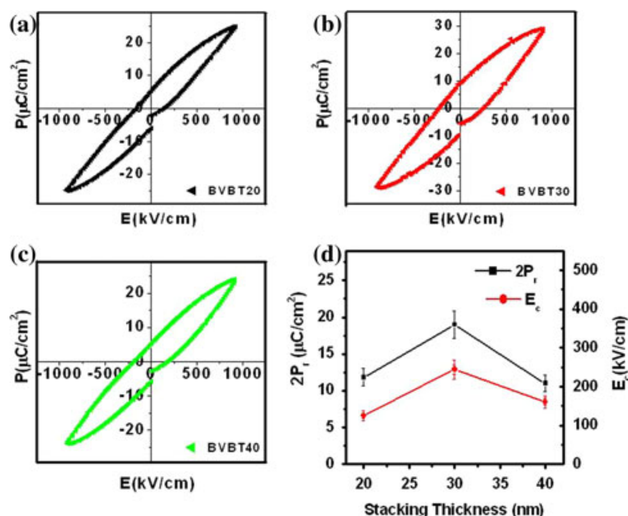

Fig. 4 **a–c** Polarization hysteresis of BVBT MLs of different stacking thicknesses. **d** Variation of remnant polarization and coercive field with stacking thickness

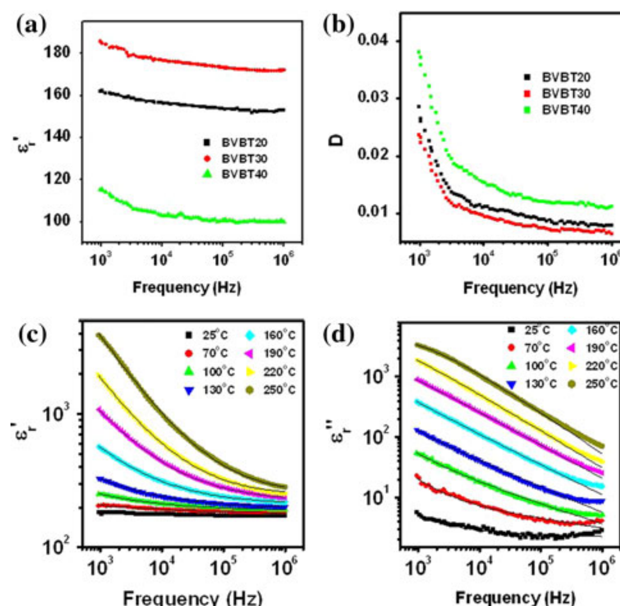

Fig. 5 **a** Room temperature dielectric constants and **b** dielectric loss of BVBT ML thin films. **c** The variation of real (ε') and **d** imaginary (ε'') part of dielectric constant as a function of frequency at various temperatures. The *solid lines* are the fittings obtained using Joncher's universal relaxation model to the experimental data

different BVBT ML films under study. The values E_c were quite different for MLs of different stacking thicknesses. For example, the $2P_r$ value for BVBT20 was $\sim$11.2 μC/cm^2 and the E_c was 155 kV/cm, whereas the same for BVBT40 were 11 μC/cm^2 and 183 kV/cm, respectively. Further $2P_r \sim 20$ μC/cm^2 and $E_c \sim 250$ kV/cm were obtained for BVBT30 ML thin film. The maximum value of remnant polarization was observed for BVBT30 ML thin film. This behavior is more evident in Fig. 4d where individual layer thickness dependence of polarization from $E = \pm 920$ kV/cm loops is plotted. It is informed from theses data that the remnant polarization is stacking thickness dependent. At a stacking thickness of 20 nm, the system exhibited a slim hysteresis loop with a maximum polarization (P_{max}) of 25 μC/cm^2. On increasing the stacking thickness, which in a way means to increase the individual layer thickness in these MLs, the P_{max} and P_r increase and reached maximum at the stacking thickness of 30 nm, and then decreased.

3.3 Dielectric behavior

Figure 5a shows the room temperature dielectric constant of BVBT MLs as a function of stacking thickness in the 100 Hz–1 MHz frequency range. The value of ε_r' was the highest for BVBT 30 ML with a stacking periodicity of 30 nm thin film. For epitaxial thin films, the dielectric constant enhancement is generally associated with increase in dielectric loss and the stacking periodicity in which the enhancement can be observed is often small (less than 10 nm). Since the ML thin films fabricated in the present study are overall polycrystalline in nature it is reasonable to assume that the thickness of interface layer is larger than that in epitaxial dielectric multilayer, which may cause the larger stacking thickness required for observing the dielectric enhancement. The nature of interface layer may also cause a difference in the dielectric behavior of these films. The variation in dielectric loss for various stacking periodicities is shown in Fig. 5b. The losses associated with the ML thin films remained low as compared to that of the pure single layer BVO thin films.

To investigate into the dielectric relaxation behavior in BVBT ML thin films, the dielectric studies were carried out in a wide range of frequencies (100 Hz–1 MHz) and temperatures (25–350 °C). The dielectric behavior of these ML films was similar except a small difference in the values. Therefore the dielectric relaxation of the representative BVBT30 ML is discussed in detail here. Figure 5c, d represents the frequency dependence of the real (ε_r') and imaginary (ε_r'') parts of the relative permittivity, at various temperatures for BVBT30 ML thin films. In these figures, the solid lines indicate the fitting of the experimental data using Joncher's model [21]. It is observed that ε_r' increases with increase in temperature, the increase being drastic at low frequency. For instance, the value of ε_r' is around 180 measured at 1 kHz and at room temperature which shoots up to around 3,900 at 250 °C. However, at higher measuring frequency, (at 1 MHz) the increase is not significant as compared to the one at low frequency i.e. the value of ε_r' increases from 170 at 25 °C to 280 at 250 °C measured at 1 MHz. This also indicates that the extent of dispersion in ε_r' increases with increase in

temperature. Further ε_r'' increases as a function of temperature and the spectral curves can be roughly separated into two regions: a low frequency part for which ε_r'' decreases strongly with increasing frequency, followed by a change in the slope of ε_r'' s the frequency is increased. The dispersion in the ε_r'' is stronger than that in the real part (Fig. 5d). This may be attributed to the influence of dc conductivity on ε_r''. The low frequency ($<10^4$) slope of the curve of ε_r'' versus frequency on log–log scale is close to −1 which is as a result of the predominance of frequency independent dc conduction in this frequency region, which overshadows the true behavior of ε_r''.

3.4 Ac conductivity analysis of BVBT30 films

As the ac conductivity has direct influence on the dielectric behavior of materials, the ac conductivity (σ_{ac}) of BVBT30 ML films has been measured as a function of frequency at different temperatures and is shown in Fig. 6a. With the increase in temperature, the dispersion and merging trend of σ_{ac} spectra at lower and higher frequencies respectively, are observed. In the mid frequencies and at high temperatures, a shoulder is observed in the σ_{ac} plot. At low temperature, the σ_{ac} increased significantly with the measuring frequency whereas at higher temperatures the variation is not that sharp. There is an overall increase in σ_{ac} with increase in temperature. Also at a constant temperature, the σ_{ac} slightly increases on high frequency side. A convenient formalism to investigate the frequency behavior

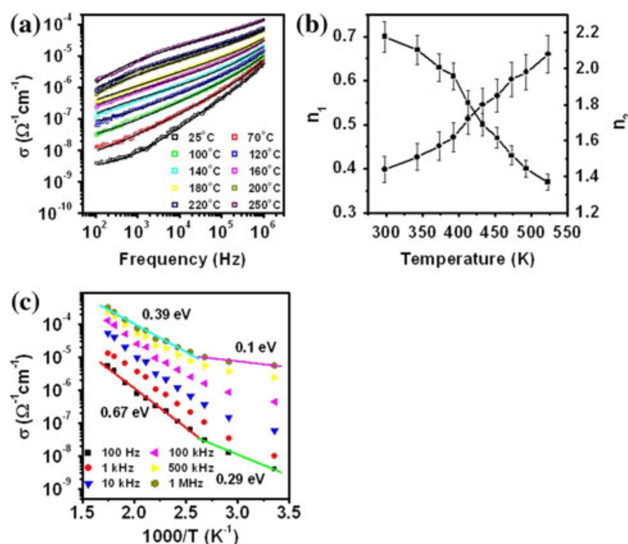

Fig. 6 **a** Frequency dependence of the ac conductivity at different temperatures for BVBT30 ML thin film. The *solid lines* indicate the double power law fits. **b** An identification of the two curves. Variation of double power law exponents (n_1, n_2) as a function of temperature (The *lines* are for guiding the eye). **c** Relation between the ac conductivity and *1000/T* (i.e. Arrhenius plot) at different frequencies for BVBT30 ML thin film

of σ_{ac} in a variety of materials is based on the power law relation proposed by Joncher [21]. In the present study, the variation of σ_{ac} of BVBT ML did not follow this relation, especially at low frequencies. Actually two different kinds of relaxations in these samples with increase in frequency are encountered:

(1) The low frequency dispersion is associated with the grain boundary/interfacial effects (large capacitance value)
(2) The high frequency one is with the grains (smaller capacitance value).

The above-mentioned observations in the σ_{ac} spectra of BVBT30 ML system have been rationalized on the basis of jump relaxation (JR) model [22] and conduction through grain boundaries and interfaces between individual BVO and BTO layers. The slower dependence of σ_{ac} on frequency at higher temperatures could be attributed to the long range translation motion of ions contributing to dc conductivity as observed in PZT-CFO multilayer structure by Ortega et al. [23]. According to JR model, the σ_{ac} in the low frequency region is associated with the successful hops to its neighborhood vacant sites due to the available long time period. Such successful jump results in a long range translational motion of ions contributing to dc conductivity. At high frequency ($>10^4$ Hz), two competing relaxation processes take place simultaneously

(1) the jumping ion may jump back to its initial position (correlated forward backward forward), i.e. unsuccessful hopping and
(2) the neighboring ion becomes relaxed with respect to the ion's position i.e. a successful hop. The increase in the ratio of the successful to unsuccessful hopping results in a more dispersive conductivity at higher frequencies.

On the lines of JR model the conductivity data for BVBT30 ML system has been fitted to a double power law relation [22, 24]

$$\sigma(\omega) = \sigma(0) + A_1\omega^{n_1} + A_2\omega^{n_2} \qquad (1)$$

The first term $\sigma(0)$ corresponds to the dc conductivity in the long time. The second term $A_2\omega^{n_1}$ is assigned to the middle region in which the exponent $0 < n_1 < 1$ characterizes the low frequency region and corresponds to the short rang translational hopping motion. The third term corresponds to the high frequency region for which the exponent $0 < n_2 < 2$ corresponds to a localized or reorientational hopping motion. The corresponding fitted results according to Eq. 1 obtained for BVBT30 ML are shown as the solid lines in Fig. 6a. This is overall related to the dispersion between relaxation of grain, grain boundaries and the interfacial polarization species. The conductivity at a

higher temperature is mainly activated by increasing temperature and the dc conductivity dominates.

The n_1 and n_2 values obtained from the fitted data for BVBT30 ML thin films have been plotted as a function of temperature in Fig. 6b. The values for n_1 and n_2 varied between 0.37–0.7 and 1.44–1.98, respectively. The n_1 values show a continuous decrease with temperature, the decrease in values being sharp in 100–250 °C. The n_2 values show a continuous increase in the measured temperature range. The crossover temperature range for n_1 and n_2 indicates the switching over from the grain contribution to the grain boundary contribution as will be discussed in the impedance and modulus analysis in the following section. Although Joncher's universal formalism [21] of dielectric relaxation suggests that the values of the exponent n should lie in the range of $0 < n < 1$, many researchers have reported [23, 24] different hopping mechanisms and these mechanisms predict a different temperature and frequency dependence of the exponent n. For BVBT30 ML thin films, we have obtained the value of n_1 less than 1 which continuously decreases with temperature. Therefore the conduction in low frequency region is attributed to the short range translational hopping assisted by large polaron mechanism. On the other hand in the case of n_2, the values are found to vary between 1.4 and 2 and increases with increasing temperature. In this case the conduction is ascribed to the localized orientational hopping assisted by small polaron hopping mechanisms [24, 25]. In the case of BVBT ML thin films, the high frequency related localized orientation hopping may be attributed to the formation of dipoles due the coexistence of the two different FE materials at the interfaces of the ML structure resulting in Maxwell–Wagner-type polarization. Also in this multilayer structure, there is a high chance of oxygen ion vacancy formation due to the vanadium present in one of the individual layers which may also trigger localized hopping mechanism.

The thermal activation of the charge species contributing to σ_{ac} at higher temperature in the whole range of frequency is further explored by the Arrhenius plots at different temperatures as depicted in Fig. 6c. The activation energies for conduction, (E_{cond}) for BVBT30 ML thin films were obtained at different frequencies and temperatures. At low frequency (100 Hz), two different values of the activation energy were obtained in two different temperature ranges. In this case at low temperature the value of $E_{cond} \sim 0.29 \pm 0.02$ eV was obtained whereas at higher temperature the value obtained was 0.67 ± 0.03 eV. The lower value of E_{cond} ($\sim$0.29 eV) might correspond to the hopping of charges between localized states where as the higher value (i.e. 0.67 eV) obtained on the high temperature side is assigned to the motion of oxygen vacancies in bismuth layered FE structures. Oxygen vacancies present in BVO and BTO are believed to create charge carriers via a defect compensation mechanism which plays an important role in resistance and dielectric degradation. In the high temperature region, the activation energy varied from 0.39 to 0.67 eV for BVBT30 ML thin film at different frequencies, and the activation energy at the lowest frequency. This frequency dependent activation energy results from the multiple site hopping conduction mechanism and this trend of decrease in activation energy with increase in frequency is observed in the entire temperature range although the change is small at lower temperature. When the temperature is increased, the localized charge carriers at each atomic site jump to another site by thermal energy on complete random base. Each site behaves as a potential well and has its own time constant of transition and the time constant (inverse of frequency of response) for the transition across a higher energy barrier (higher activation energy) is large as compared to that across the smaller ones. Therefore the traps with high activation energy respond at lower frequency and vice versa. This gives rise to the frequency dependent activation energy in these samples.

3.5 Impedance analysis

Impedance spectroscopy studies of BVBT ML thin films have been carried out in order to establish the correlation between the microstructure and electrical properties. The variation of Z'' as a function of frequency for BVBT30 ML is shown in Fig. 7 for low (a) and high (b) temperature range. Here Z'' is plotted on log scale to have the clear insight into its behavior. This ML structure exhibited a high value of impedance at low temperature, and then at temperatures >140 °C, a second region appeared. In Fig. 7a, a weak peak around 10^4 Hz appeared which shifted towards higher frequency with decreased intensity as the temperature increased. This is more clearly seen in Fig. 7b as indicated by an arrow. A second peak appeared at much higher temperature at lower frequency side. This phenomenon was seen more clearly on Nyquist plots of BVBT

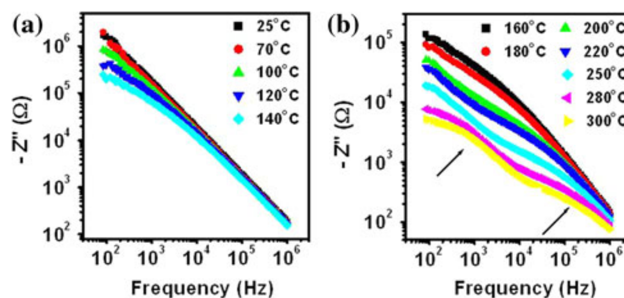

Fig. 7 Frequency dependence of the imaginary part of impedance (Z'') for BVBT30 ML thin film: **a** At relatively low temperatures and **b** at elevated temperatures

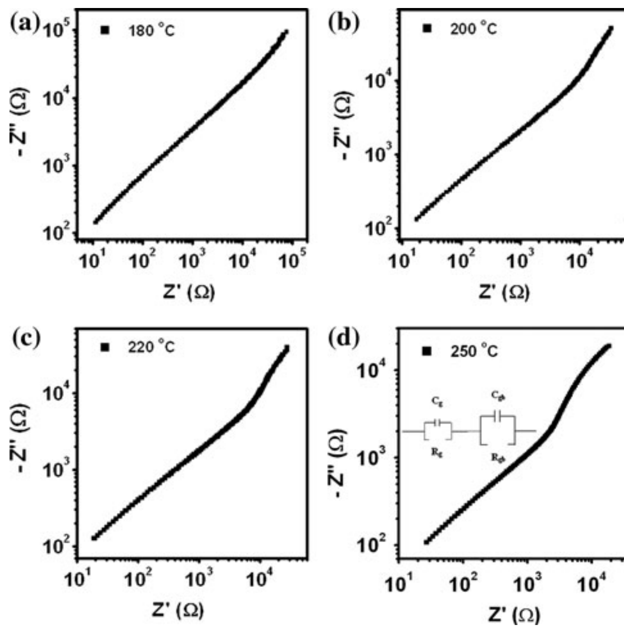

Fig. 8 a–d Complex impedance plots (Z′ vs. Z″) for BVBT30 ML thin film at various temperatures. Inset in **d** represents the RC equivalent circuit used to describe the electrical properties

ML film (Fig. 8a–d) at four different temperatures. At low temperature, one straight line was observed which indicates the response of the bulk/grains in BVBT ML thin film. However at higher temperatures another arc appeared at low frequency side which might be due to the grain boundaries/interfacial polarization in ML films. To analyze further the impedance data was modeled by an ideal equivalent circuit comprising of resistance, *R* and capacitance, *C*. In the present case, the polycrystalline ML thin films generally show intergranular or grain boundary/interfacial impedances, the overall BVBT ML thin film system could be represented by a series combination of two parallel RC elements given in the inset of Fig. 8d, each representing the contributions from grain interiors and grain boundaries/interfacial regions, respectively. Each region can be realistically described by a parallel combination of a capacitor and a resistor. Taking (R_g, R_{gb}) and (C_g, C_{gb}) as the resistances and capacitances of the grain and grain boundaries, respectively, we obtain

$$Z' = \frac{R_g}{1 + (\omega R_g C_g)^2} + \frac{R_{gb}}{1 + (\omega R_{gb} C_{gb})^2} \quad (2)$$

$$Z'' = R_g\left[\frac{\omega R_g C_g}{1 + (\omega R_g C_g)^2}\right] + R_{gb}\left[\frac{\omega R_{gb} C_{gb}}{1 + (\omega R_{gb} C_{gb})^2}\right] \quad (3)$$

Based on Eq. 3, the response peaks of grains and grain boundaries are located at $1/(2\pi(R_gC_g))$ and $1/(2\pi(R_{gb}C_{gb}))$, respectively and the peak values are proportional to the associated resistances. In general, peak frequency for grain boundaries was much lower than that of grains due to their large resistance and capacitance as compared to those of grains. Therefore, in the impedance spectra, the higher frequency response i.e. the straight line in Fig. 8 is attributed to the grains, and the arc at lower frequency to the grain boundaries. Comparing the values of the two responses, it was found that even at an elevated temperature (250 °C), the resistance of grain boundaries is at least one order of magnitude larger than that of grains i.e., $R_{gb} > R_g$. Since the grain boundary response in BVBT30 ML was not fully evolved due to the temperature and frequency limitations, the modulus formalism was used to have an insight into the smaller capacitance entities in BVBT MLs.

3.6 Modulus formalism

It is well known that the smaller capacitance value dominates in the electric modulus spectra, which magnify the grain effects making them easier to analyze. In order to analyze the grain effect in BVBT30 ML thin films in detail, the modulus formalism was employed to discuss the results. The complex modulus plots obtained for BVBT30 ML thin film have been shown in Fig. 9 at four different temperatures. One semicircle was observed at low temperature (220 °C) whereas symptoms of the appearance of second semicircle at relatively higher temperature (∼250 °C) were seen. The first semicircle represents the capacitive grain boundary effects in the high temperature and low frequency regime and the second one represents the capacitive grain effects at elevated temperatures. The magnitude of the well resolved large semicircle at low temperatures decreased with the increase of temperature. Further the grain boundary response in BVBT ML thin film appeared only after a

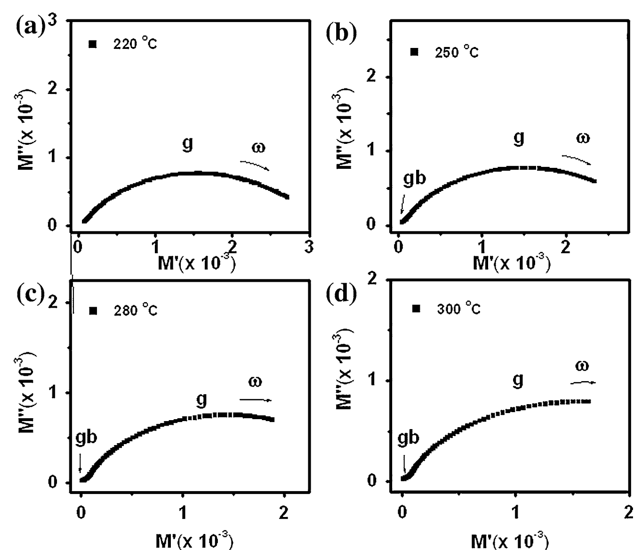

Fig. 9 Complex electric modulus plane plots (M′ vs. M″) at different temperatures for BVBT 30 ML thin film

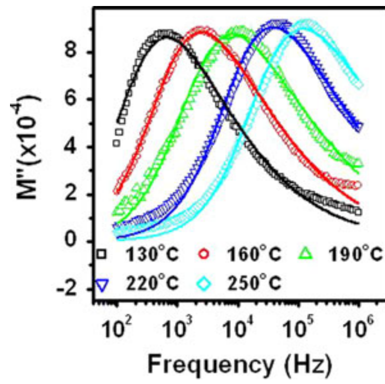

Fig. 10 The variation of the imaginary part of the electric modulus (M″) as a function of frequency for BVBT30 ML thin film at various temperatures

particular temperature (>200 °C) while the grain response remains there in the same temperature. The grain and grain boundary capacitances were weakly temperature dependent. Also the magnitude of grain boundary in case of BVBT30 ML thin film was roughly ten times the magnitude of the grain capacitance (Fig. 9).

The variation of imaginary part of modulus (M'') as a function of frequency for BVBT30 ML thin films has been depicted in Fig. 10 at various temperatures. The imaginary part of the electric modulus indicates the energy loss under electric field. Similar to the impedance formalism, the response of the grains could be captured clearly for BVBT30 ML thin films. The peak position of response frequencies in (M'') versus frequency for the grain effect shifted rapidly towards the higher frequency side with the increase in temperature. This indicate the involvement of temperature-dependent relaxation processes in the present multilayer thin films. The frequency region below the M″ peak might be the range in which the charge species drift to long distances. In the frequency range above the peak, the ions/vacancies could be spatially connected to potential wells and free to move only within the wells. The frequency range where the peaks occur is suggestive of the transition from long-to short-range mobility. The modulus data was further analyzed by using the macroscopic decay function to calculate the electrical modulus [26]. The electric modulus behavior of the BVBT30 Ml thin films was rationalized by invoking the modified Kohlrauschn-Williamsn-Watts (KWW) function as suggested by Bergman [26, 27]:

$$M''(\omega) = \frac{M_{\max}}{(1-\beta) + \frac{\beta}{1+\beta}\left[(\omega_{\max}/\omega + \omega_{\max}/\omega)^{\beta}\right]} \quad (4)$$

where $M''_{\max}$ is the peak M'', and $\omega_{\max}$ is the corresponding frequency, β is the stretched exponent parameter $(0 < \beta < 1)$ and it characterizes the deviation from the ideal Debye-type relaxation. The above Eq. 4 could effectively be described for $\beta \geq 0.4$. The theoretical fit of Eq. 4 to the experimental data has been shown in Fig. 10 as the solid lines. It is observed that the experimental data are well fitted to this model, except the high frequency data for low temperature and the low temperature data for the high temperature. This might be due to the fact that the grain response shifts towards higher frequency at higher temperature and the grain boundary response just starts appearing at low frequency and at higher temperature. It may be seen that at higher temperature, the overall response could not be described by only one component in Eq. 4. However the grain boundary response was not fully evolved in the present case, so it could not modeled appropriately. From the fitting of M'' versus frequency plots, for BVBT30 ML thin film, the value of β was found to be 0.4262 ± 0.0001 to 0.4561 ± 0.0001 in 140–300 °C temperature range. This value is a measure of the strength of cation–cation interactions, and it could vary with the number of cations available for conduction. In the present study, the value of β increased from 0.42 to 0.45 in the 140–300 °C temperature range. Therefore β increased as the interaction among mobile charge carriers decreased, resulting in the increase in conductivity at higher temperatures [26].

Figure 11a show the normalized plots of electric modulus M'' versus frequency, where the frequency has been scaled by the peak frequency. A perfect overlapping of all the curves on a single master curve was found. This time–temperature superimposition suggests that the conduction mechanism remains unchanged. The relaxation time (τ) associated with the process was determined from the plot of M'' versus frequency. The fitted τ values follow the Arrhenius law of thermal activation process. The activation energy involved in the relaxation process of ions was obtained from the temperature-dependent relaxation time

$$\tau = \tau_o \exp\left(\frac{E_R}{kT}\right) \quad (5)$$

where E_R is the activation energy associated with the relaxation process, τ_o is the pre-exponential factor, k is the Boltzmann constant, and T is the absolute temperature.

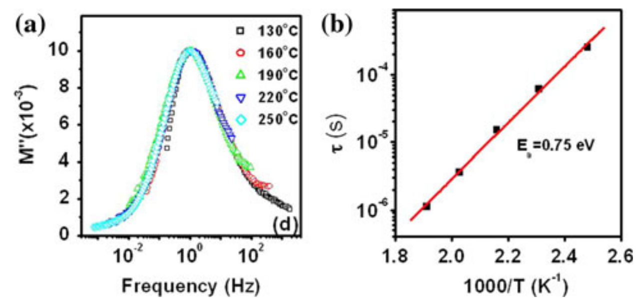

Fig. 11 **a** Normalized master plots of electric modulus versus normalized frequency for BVBT30 ML film. **b** Variation of dielectric relaxation time (τ) with the reciprocal of temperature (1000/T)

Figure 11b shows a plot between $ln\ \tau$ and1000/T along with the theoretical fit (solid line) to the above Eq. 5. The value obtained for E_R is 0.75 ± 0.03 eV which can be ascribed to the motion of oxygen ion vacancies in these ML thin films. This value of activation energy agrees well with that obtained from ac conductivity analysis of these films.

4 Conclusions

In summary, the $Bi_2VO_{5.5}/Bi_4Ti_3O_{12}$ multilayer thin films with different individual layer thickness were successfully fabricated on platinized silicon substrate with multi target pulsed laser deposition technique. The XRD studies confirmed the phase purity comprising both the starting materials. The atomic force microscopy studies showed that the films were smooth with rms roughness of ~4–5 nm for all films. The cross sectional SEM studies indicated a dense microstructure and the thickness of the films were ~350 nm for all samples studied. The maximum remnant polarization was observed for BVBT30 ML thin film ($2P_r \sim 20\ \mu C/cm^2$ and $E_c \sim 232$ kV/cm). The maximum dielectric constant (~170) was observed for BVBT30 ML thin films among the sample studied here. Further, the frequency and temperature dependence of the dielectric, impedance, modulus and conductivity spectra of these films were investigated in detail. The dielectric data was modeled according to Joncher's universal relaxation. We observed two different conduction processes in impedance and modulus spectra attributed to grain and grain boundary effects, although the later was not fully evolved in the measured frequency and temperature range. A deviation from the Debye type relaxation was observed from the impedance studies. The stretching exponent, β calculated from the fitting of the modulus spectra slightly dependent on temperature indicating grain boundary dependent conductivity at elevated temperatures. The ac conductivity was found to obey well the double power law, indicating the different contribution to the conductivity, the low frequency conductivity being due to the short range translational hopping and the high frequency conductivity is due to the localized or reorientational hopping motion.

References

1. G. Rijnders, D.H.A. Blank, Nature **433**, 369 (2005)
2. J.B. Neaton, K.M. Rabe, Appl. Phys. Lett. **82**, 1586 (2003)
3. K. Ueda, H. Tabata, T. Kawai, Science **280**, 1064
4. D.P. Norton, B.C. Chakoumakos, J.D. Budai, D.H. Lowdes, B.C. Sales, J.R. Thompson, D.K. Christen, Science **265**, 2704 (1994)
5. G.Q. Gong, A. Gupta, G. Xiao, P. Lecouer, T.R. Mcguire, Phys. Rev. B **54**, R3742 (1996)
6. P. Murugavel, D. Saurel, W. Prellier, C. Simon, B. Raveau, Appl. Phys. Lett. **85**, 4424 (2004)
7. K.B.R. Varma, G.N. Subbana, T.N. Guru Row, C.N.R. Rao, J. Mater. Res **5**, 1 (1991)
8. V.G. Osipian, L.M. Savchenk, V.L. Elbakyan, P.B. Avakyan, Inorg. Mat. **23**, 467 (1987)
9. V.N. Borisov, M.Y. Poplavko, P.B. Avakyan, V.G. Osipyan, Sov. Phys. Solid State **30**(5), 904 (1988)
10. K.V.R. Prasad, K.B.R. Varma, J. Phys. D Appl. Phys. **24**, 1858 (1991)
11. F. Abraham, M.F. Debreuille Gresse, G. Mairesse, G. Nowogrocki, Solid State Ionics **28–30**, 529 (1990)
12. B.H. Park, B.S. Kang, S.D. Bu, T.W. Noh, J. Lee, W. Jo, Nature (London) **401**, 682 (1999)
13. H. Maiwa, N. Lizawa, D. Togawa, T. Hayashi, W. Sakamoto, M. Yamada, S. Hirano, Appl. Phys. Lett. **82**, 1760 (2003)
14. T. Watanabe, H. Funakubo, M. Osada, Y. Noguchi, M. Miyayama, Appl. Phys. Lett. **80**, 100 (2002)
15. A.D. Rae, J.G. Thompson, R.L. Withers, A.C. Willis, Acta Crystallogr. Sec. B Structr. Sci. **46**, 474 (1990)
16. K.V.R. Prasad, Ph.D Thesis, 160, Indian Institute of Science, 1994
17. N. Kumari, S.B. Krupanidhi, K.B.R. Varma, Mater. Sci. Eng. B **138**, 22 (2007)
18. P.C. Joshi, S.B. Krupanidhi, Appl. Phys. Lett. **62**, 1928 (1993)
19. P.C. Joshi, S.B. Krupanidhi, A. Mansingh, J. Appl. Phys. **72**, 5517 (1992)
20. G.W. Pabst, L.W. Martin, Y.-H. Chu, R. Ramesh, Appl. Phys. Lett. **90**, 072902 (2007)
21. A.K. Joncher, *Dielectric Relaxation in Solids* (Chelsea Dielectric Press, London, 1983)
22. K. Funke, Prog. Solid St. Chem. **22**, 111 (1993)
23. N. Ortega et al., Phy. Rev. B **77**, 014111 (2008)
24. A. Pelaiz-Barramco, M.P. Gutierrez-Amador, A. Huanosta, R. Valenzuela, Appl. Phys. Lett. **73**, 2039 (1998)
25. A.A.A. Youssef, Z. Naturforsch, A Phys. Sci. **57**, 263 (2002)
26. R. Bergman, J. Appl. Phys. **88**, 1356 (2000)
27. G. Williams, D.C. Watts, Trans. Faraday Soc. **66**, 80 (1970)